ADVANCED MATERIALS
www.advmat.de

Proton-Conductive Melanin-Like Fibers through Enzymatic Oxidation of a Self-Assembling Peptide

Samala Murali Mohan Reddy, Eileen Raßlenberg, Sian Sloan-Dennison, Travis Hesketh, Ohad Silberbush, Tell Tuttle, Ewen Smith, Duncan Graham, Karen Faulds, Rein V. Ulijn, Nurit Ashkenasy,* and Ayala Lampel**

Melanin pigments have various properties that are of technological interest including photo- and radiation protection, rich coloration, and electronic functions. Nevertheless, laboratory-based synthesis of melanin and melanin-like materials with morphologies and chemical structures that are specifically optimized for these applications, is currently not possible. Here, melanin-like materials that are produced by enzymatic oxidation of a supramolecular tripeptide structures that are rich in tyrosine and have a 1D morphology are demonstrated, that are retained during the oxidation process while conducting tracks form through oxidative tyrosine crosslinking. Specifically, a minimalistic self-assembling peptide, Lys–Tyr–Tyr (KYY) with strong propensity to form supramolecular fibers, is utilized. Analysis by Raman spectroscopy shows that the tyrosines are pre-organized inside these fibers and, upon enzymatic oxidation, result in connected catechols. These form 1D conducting tracks along the length of the fiber, which gives rise to a level of internal disorder, but retention of the fiber morphology. This results in highly conductive structures demonstrated to be dominated by proton conduction. This work demonstrates the ability to control oxidation but retain a well-defined fibrous morphology that does not have a known equivalent in biology, and demonstrate exceptional conductivity that is enhanced by enzymatic oxidation.

Melanins are natural pigments that serve a range of aesthetic,[1] electric,[2–4] and protective functions, including photo[5] and radioprotection,[6] and have for this reason generated interest for potential technological applications. The most abundant type of melanin found in nature, eumelanin, is produced by enzymatic oxidation of tyrosine into 3,4-dihydroxyphenylalanine (DOPA) and further oxidation products that subsequently polymerize to form the pigment.[7] The oligomerization and polymerization is not well understood and the heterogeneity and disorder of the polymer renders its structural and chemical characterization extremely challenging. As a result, there is still only incomplete fundamental understanding of its structure, which restricts the ability to rationally optimize and repurpose the material for applications.[8] These challenges have inspired efforts to design synthetic mimics, that are typically produced by the oxidation of dopamine into

Dr. S. M. M. Reddy, O. Silberbush, Prof. N. Ashkenasy
Department of Materials Engineering and Ilse Katz Institute for Nanoscale Science and Technology
Ben-Gurion University of the Negev
P.O.B. 653, Beer-Sheva 84105, Israel
E-mail: nurita@bgu.ac.il

E. Raßlenberg
Organisch-Chemisches Institut
University of Muenster
Corrensstraße 40, Muenster 48149, Germany

Dr. S. Sloan-Dennison, T. Hesketh, Prof. T. Tuttle, Prof. E. Smith, Prof. D. Graham, Prof. K. Faulds
Department of Pure and Applied Chemistry
Technology and Innovation Centre
University of Strathclyde
Glasgow G1 1XL, UK

Prof. R. V. Ulijn, Dr. A. Lampel
Advanced Science Research Center (ASRC) at the Graduate Center
City University of New York (CUNY)
85 St Nicholas Terrace, New York, NY 10031, USA
E-mail: rulijn@gc.cuny.edu

The ORCID identification number(s) for the author(s) of this article can be found under https://doi.org/10.1002/adma.202003511.

DOI: 10.1002/adma.202003511

Prof. R. V. Ulijn
Department of Chemistry
Hunter College
City University of New York
695 Park Avenue, New York, NY 10065, USA

Prof. R. V. Ulijn
Ph.D. programs in Biochemistry and Chemistry
The Graduate Center of the City
University of New York
New York, NY 10016, USA

Dr. A. Lampel
The Shmunis School of Biomedicine and Cancer Research
George S. Wise Faculty of Life Sciences
Tel Aviv University
Tel Aviv 69978, Israel
E-mail: ayalalampel@tauex.tau.ac.il

Dr. A. Lampel
Sagol Center for Regenerative Biotechnology
Tel Aviv University
Tel Aviv 69978, Israel

Dr. A. Lampel
The Center for Nanoscience and Nanotechnology
Tel Aviv University
Tel Aviv 69978, Israel

polydopamine or similar polymers.[1,9] While these materials show optical and electrical properties that resemble those of natural melanins, their chemical structure and nano/micrometer-scale morphology cannot be easily regulated, forming spherical structures composed of polymers with compositions that are not fully understood.[7,8]

One of the most studied properties of melanin, and more specifically eumelanin, is its featureless and broadband absorption,[10] which has been related to the conjugated nature and chemical and structural disorder of the material.[11] The broadband absorption also dictates the electronic properties, which have been the subject of extensive research over the years.[2,12–14] It is widely accepted that the conductivity of melanin and melanin-like materials is strongly controlled by internal structural disorder.[8,11] However, the type of charge carriers (electrons or protons) of these melanin-like materials and the mechanisms of charge transport are not yet clear.[10,12–17] Furthermore, optimization of the materials in terms of hierarchical structure and chemical organization for improved conductivity, has been challenging, and to the best of our knowledge, has not yet been addressed, thus limiting application of these structures in bioelectronics.

Supramolecular self-assembly of short peptides is an attractive approach for construction of materials with structural and morphological properties that are defined across the molecular to the nano- and micrometer scale.[18–20] We have previously reported on the formation of melanin-like materials by using self-assembling tyrosine-tripeptides that pre-organize tyrosine side chains within supramolecular fibrous structures, which in turn serve as supramolecular substrates for enzymatic oxidative polymerization of tyrosine. Using a number of sequence isomers of peptides composed of tyrosine, phenylalanine, and aspartic acid, we could demonstrate that the peptide sequence dictates the self-assembly properties, and furthermore upon enzymatic oxidation provides access to a range of pigment materials with properties that are directly related to the self-assembly properties of the precursors.[21] Building on this previous work, we hypothesized that by stabilizing the 1D supramolecular form of the peptide, subsequent oxidation could give rise to formation of conductive tracks through chemical oxidation of pre-organized tyrosines, while retaining the overall fibrous morphology, that in turn would improve the electric properties of the films.

Informed by our previously reported design rules for self-assembling tripeptides,[22] and recognizing the high prevalence of lysine in natural DOPA-containing proteins and its contribution to self-assembly,[23,24] we selected a self-assembling peptide precursor composed of lysine–tyrosine–tyrosine (KYY). We hypothesized that two tyrosine molecules within the tripeptide precursor, will facilitate the formation of pigment while retaining fiber morphology following oxidation. This is due to stabilization of the peptide self-assembled structure through π–π stacking, cation–π interactions with the lysine side chain,[23] and intermolecular crosslinking between adjacent oxidized phenols (**Figure 1**A).

The tripeptide self-assembled (aqueous solution at pH 7.5) into a suspension containing nano- and micrometer scale fibers (Figure 1A,B). Following enzymatic oxidation using tyrosinase (0.2 mg mL^{-1}), a color change to brown was observed after 24 h (Figure 1A). Optical microscopy analysis showed that oxidized KYY assemblies $(KYY)_{ox}$ retain their fibrillar morphology (Figure 1B, bottom). Scanning and transmission electron microscopy (SEM, TEM) analyses confirmed that the fibers retain their morphology at the nanoscale following oxidation (Figure 1C,D). This is in contrast to the previously reported peptide fibers formed by the peptide DYF which did not retain a 1D morphology and reconfigured to spherical structures upon oxidation. The previously reported peptide YFD showed

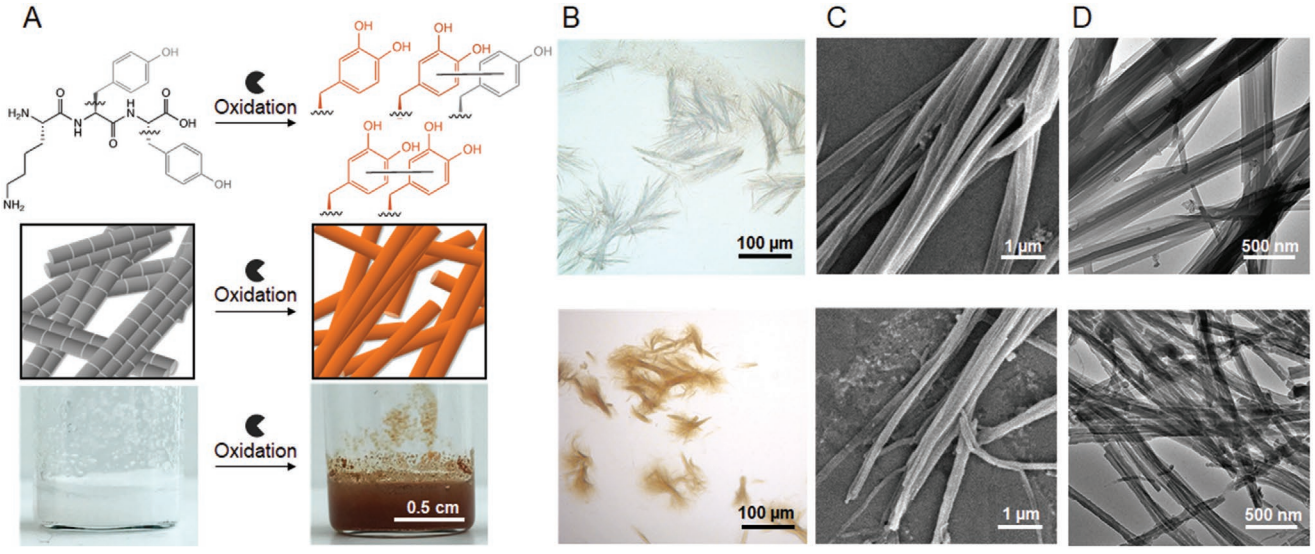

Figure 1. Structure and morphology of melanin-like peptide nanofibers. A) Chemical structures of KYY (tyrosine side chain in gray) and its oxidized side chains (indicated in orange) with schematic representation of the melanin-like nanofibers formed by enzymatic oxidation of assembled fibers below. Macroscopic images of the materials formed by self-assembly of KYY (aqueous solution, pH 7.5) and following enzymatic oxidation (0.2 mg mL^{-1} tyrosinase) for 24 h is shown at the bottom. B) Optical microscopy, C) SEM, and D) TEM images of KYY and $(KYY)_{ox}$ showing retention of fibrillar morphology at the nanoscale.

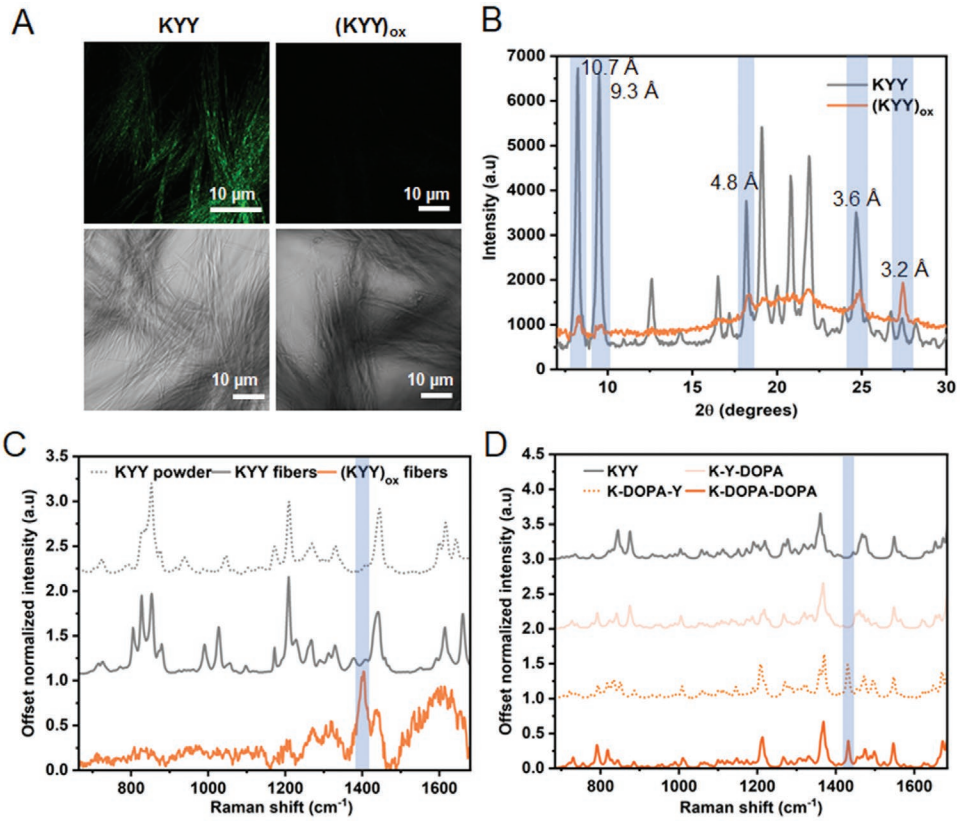

Figure 2. Characterization of structure and supramolecular organization of melanin-like nanofibers. A) SHG two-photon images (top) and confocal bright-field images (bottom) of KYY (left) and $(KYY)_{ox}$ (right) fibers. B) WAXS analysis of KYY (gray) and $(KYY)_{ox}$ (orange) with specific *d*-spacing indicated in light blue. C) Raman spectra of KYY unassembled powder (dotted gray), KYY fibers (gray), and $(KYY)_{ox}$ fibers (orange). D) DFT calculations of KYY and $(KYY)_{ox}$ vibration spectra at different oxidation levels. Raman shift at 1400 cm^{-1} (blueshifted to 1430 cm^{-1} in the calculations) indicative of phenol oxidation is highlighted in light blue in (C) and (D).

retention of fibrillar morphology but only low enzymatic conversion yield.[21] We note that the replacement of aspartic acid with lysine (in KYF), alone, was also found to be insufficient for stabilizing the nanofiber morphology following enzymatic oxidation, resulting the formation of spherical particles (Figure S1, Supporting Information).

Second-harmonic generation (SHG) microscopy analysis of KYY fibers showed two-photon emission arising from their noncentrosymmetric crystallinity (**Figure 2**A).[25] This signal disappeared following fiber oxidation, indicating the partial loss of internal supramolecular order upon oxidation while the overall fiber morphology was clearly retained. To analyze the level of disorder of the fibers structure following oxidation, we used powder wide-angle X-ray scattering (WAXS) analysis. KYY fibers showed high crystallinity (Figure 2B), with specific *d*-spacings indicating that the molecules interact through H-bonding of the peptide backbone to form a β-sheets packing[26] (10.7, 9.3, 4.8 Å) and π–π-stacking interactions between aromatic side chains (3.6 Å). Following oxidation, the crystallinity of the fibers decreased, as evident by the lower signal (Figure 2B) and in agreement with the SHG analysis. This is in contrast to the complete loss of signals associated with β-sheets packing and π–π-stacking for previously reported tyrosine-tripeptides upon oxidation that did not retain their shape.[21] The fact that the X-ray signal was not entirely lost (Figure 2B) provides evidence of some retention of supramolecular order within the oxidized fibers. The partial retention of β-sheet-like conformations and π–π-stacking interactions upon oxidation suggests that retention of H-bonding stabilization is responsible for retention of fibrillar morphology.

Liquid chromatography–mass spectrometry (LCMS) of the solution fraction of $(KYY)_{ox}$ indicated the oxidation of phenol groups to DOPA (Figure S2, Supporting Information). UV–vis absorbance analysis showed the depletion of the phenol absorbance peak at 277 nm over time following oxidation and the simultaneous emergence of broadband absorbance between 300–600 nm, which is typical for the oxidation and polymerization of the phenol groups to form conjugated oligomeric species (Figure S3, Supporting Information).

Vibrational Raman spectroscopy was used to gain additional insights into the chemical changes within the fibers upon oxidation (Figure 2C). Changes in the spectra observed upon fiber assembly compared to the unassembled KYY powder confirm the formation of an ordered supramolecular system. For example, the distinctive tyrosine doublet at 852 cm^{-1} and 830 cm^{-1} originating from two independent fundamental modes of the phenol ring, in-plane or out of plane, appeared in the KYY powder spectra.[27] However, upon fiber formation, four defined peaks were found at 806, 830, 852, and 882 cm^{-1}, suggesting that at least one, or both, of the tyrosines interact

with a backbone carbonyl group after assembly into fibers.[27] In addition, new bands at 1229 and 1661 cm^{-1} appeared following assembly. These bands are characteristic of β-sheet arrangements,[28–31] and were previously observed (at 1660 cm^{-1}) for tripeptide assemblies.[21]

A noisier Raman spectrum was obtained after enzymatic oxidation of the fibers, most likely due to self-absorption of the exciting and scattered radiation. The broad peak at about 1600 cm^{-1} suggests that amide bonds are retained but they are now exposed to different environments. Two distinctive peaks at 1400 and 1430 cm^{-1} were selectively enhanced over other peaks in the spectrum (Figure 2C). Since the sample is colored, this is likely to be due to resonance enhancement of a catechol in quinonoid form. DFT calculations were used to test this hypothesis (Figure 2D). Multiple possible oxidized forms of KYY were constructed and analyzed computationally (for details see Experimental Section). The theoretical Raman spectra was calculated for KYY and each of the possible oxidized forms of KYY, and compared to the independently obtained experimental spectra of KYY and $(KYY)_{ox}$ fibers. A peak at 1430 cm^{-1} (Figure 2D), appeared in the calculated vibrational spectra of K-DOPA-Y and K-DOPA-DOPA. This peak can be assigned to the experimentally measured peak at 1400 cm^{-1} (Figure 2C), considering the blueshift commonly observed in DFT simulations. It corresponds to an asymmetric ring stretching mode in the oxidized ring system and is therefore assigned to the oxidation of the middle tyrosine to a catechol (Figure 2D). A calculation of the KYY vibronic structure indicates that H-bonding to the oxygen in the middle catechol, when in the quinonoid form, will aid in producing a colored species. A study of the oxidation process for a related system showed that a number of colored species, based on quinonoid formation as intermediates during that reaction, were formed and that resonance Raman scattering, which has different selection rules to Raman scattering, occurs.[32] In resonance Raman scattering selected peaks are enhanced and they usually have vibrational displacements which give good electronic overlap throughout the vibrational displacement. The assignment made here complies with this condition. Thus, the complementary analyses using LC-MS, Raman spectroscopy, and DFT calculations collectively provide insights into the specific chemical groups forming following oxidation, both in the solution fraction of KYY and in the fibers.

The formation of fibrillar structures containing catechol groups with a level of directional order was expected to give rise to enhanced conductivity in the films.[14] To test the effect of oxidation on the conductivity, current–voltage (I–V) curves were obtained for KYY and $(KYY)_{ox}$, fibers under a range of relative humidity in hydrogen-rich (4.8%) atmosphere that hydrogenate the Pd metal pads to form proton transparent PdH_x contacts.[33,34] Since transient measurements have indicated possible time dependent contribution of both displacement current and contact polarization effects to the measured current (Figure S4, Supporting Information), the I–V measurements were conducted using small voltage steps of 50 mV and a 2 s sweep delay between each step to minimize as much as possible the contribution of both effects. The I–V of KYY and $(KYY)_{ox}$ showed a linear behavior between –0.5 and 5 V (**Figure 3**A,B). Slope of unity in log-log scale (Figure S5, Supporting Information) indicated Ohmic behavior at this voltage range for both samples for relative humidity conditions between 40% and 70%. We note that low electric field space charge limiting current effects are ruled out by the linear dependence of the current on the gap between the contacts that will be discussed below.

The conductance of the oxidized fibers was found to be an order of magnitude larger than that of the fibers before oxidation (Figure 3C). This increase in the conductance indicates that the formation of catechol groups significantly increases charge flow in the films. This enhancement in charge transport may be assigned to increase in the fibers' charge carriers' concentration, that is, a doping process, and/or to improved water adsorption, which would affect proton conduction in particular.

To test the importance of the fibrous morphology on charge transport, we compared the conductance of KYY and $(KYY)_{ox}$ fibers to that of films prepared from the solution fraction of $(KYY)_{ox}$ that contains $(KYY)_{ox}$ oligomers [$(KYY)_{ox\text{-}sup}$ in Figure 3C]. These experiments further confirmed the role of catechol formation on the conductance, with the conductance of $(KYY)_{ox\text{-}sup}$ film found to be larger than that of KYY films (Figure 3C). The fibrous films of $(KYY)_{ox}$ presented the highest conductance values, highlighting the importance of retention of structural order in improving charge conduction in the melanin-like materials. We note that beyond the improvement of charge transport efficiency by the retention of fibrillar morphology in the oxidized fibers, the use of ordered peptide template can influence the efficiency of oxidation and catechol formation, and the chemical structure of the polymerized products, which can also enhance the conductivity.

$(KYY)_{ox}$ fiber conductance continued to increase with oxidation time, reaching an order of magnitude increase after 4 days (Figure S6A, Supporting Information). This conductance enhancement was accompanied by bundling of the fibers (Figures S7,S8, Supporting Information). We postulate that this bundling is due to interfiber polymerization of the tyrosine side chains. It is plausible that the polymerization of side chains of different fibers aligns the fibers with respect to each other and reduce fiber to fiber resistance, improving the conductivity of the melanin-like film. Further studies, including single fiber measurements, are required in order to evaluate the relative contribution of intra and intermolecular polymerization to the conductivity of the film. Notably, $(KYY)_{ox}$ fibrillar morphology was retained even after 6 days of oxidation (Figures S7,S8, Supporting Information). In contrast, the conductance of KYY fibers (Figure S6B, Supporting Information), for which no apparent changes in films morphology were observed (Figures S7,S9, Supporting Information), remained intact.

The conductivity of the films, which was extracted from transfer line measurement (TLM) curves (Figures S10,S11, Supporting Information),[35–37] increased exponentially with the humidity for both samples (Figure 3D), confirming that proton transport dominates the conductivity. We note that no current was observed for both samples under vacuum conditions (Figure S12, Supporting Information), further confirming that the flow of charge is mostly dominated by proton transfer processes.[38,39] Fiber oxidation significantly enhanced the proton conductivity, with larger differences of about three orders of magnitude at 40% relative humidity and two order of magnitude at 70% relative humidity. An in-plane conductivity value

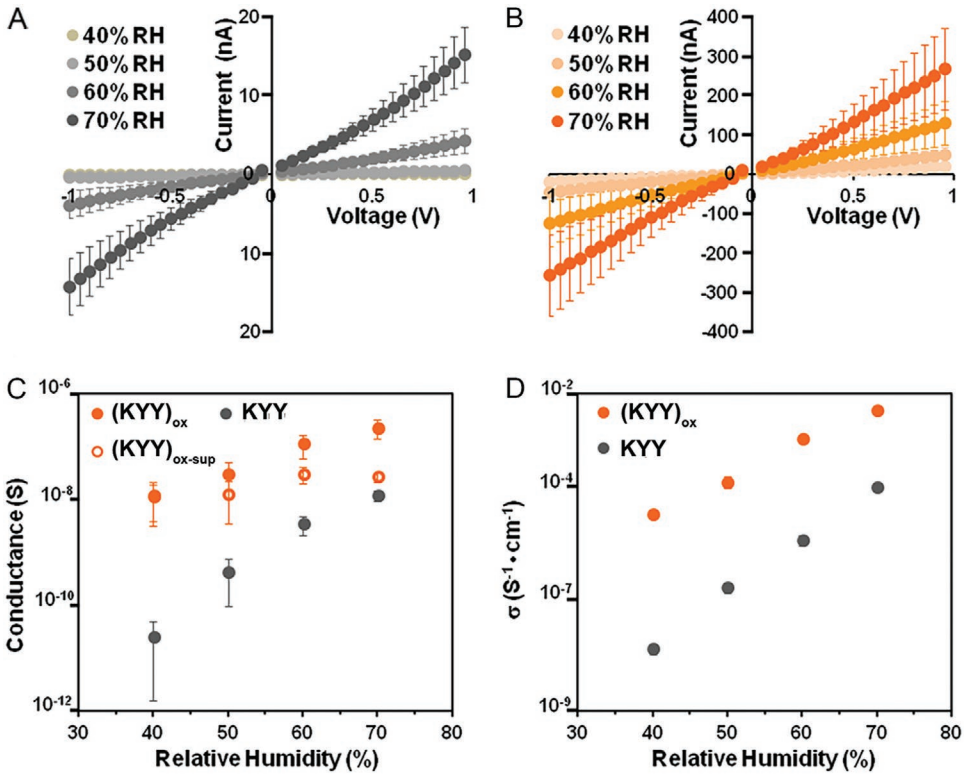

Figure 3. Electric behavior of KYY fibers before and after oxidation as a function of relative humidity. A) *I–V* curves of films of KYY fibers at different relative humidity measured with PdHx contacts with 10 µm gap. B) *I–V* curves of films of $(KYY)_{ox}$ fibers after 4 days of oxidation. C) Conductance of the KYY and $(KYY)_{ox}$ films, as well as data for a film deposited from solution fraction of the oxidized peptide: $(KYY)_{ox\text{-}sup}$, as a function of relative humidity. Conductance was calculated from the slope of the *I–V* curves. D) Conductivity of the $(KYY)_{ox}$ and KYY films as a function of relative humidity. Conductivity was extracted from TLMs (Figures S10,S11, Supporting Information) after 4 days for $(KYY)_{ox}$ fibers, and after one day equilibration in solution for KYY fibers.

of 4 mS cm^{-1} was found for the oxidized film at 70% RH. This represents an upper limit value since it was calculated considering the vertical contact cross section. While previous studies from our group indicate that this calculation closely represents the actual conductivity value,[40] we note that a more conservative estimation, taking into account the larger film cross section, yields a conductivity value of ≈0.35 mS cm^{-1}. In any case, both values represent a high in-plane conductivity, comparable to that of ultrathin films of Nafion,[40] a polymer electrolyte which is commonly used as the membrane in fuel cells.[41] This high in-plane conductivity is also similar to the out-of-plane conductivity measured for ultrathin films of synthetic melanin,[12] suggesting that the highly anisotropic fibrillar morphology, and possibly the degree of order, play a key role in maintaining high in-plane conductivity over mesoscopic distances.

The out-of-plane conductivity of the thin synthetic melanin film was assigned to proton transport.[12] This is in contrast to earlier works that have suggested the dominance of electron transport in melanins,[13,15] and studies that suggested mixed electron/proton conductivity.[10,14,16,17] Impedance spectroscopy was used as a first indication to elucidate the type of charge carriers (Figure S13, Supporting Information).[42] The shape of the Nyquist plot for both KYY and $(KYY)_{ox}$ fibers, with a semicircle at high frequencies and an inclined line at lower frequencies, is typical for proton conductors and provide no evidence for electronic contribution to the impedance. Kinetic isotope effect (KIE) experiments were used to further confirm the dominance of protons to charge transport processes for the entire relative humidity range.[40,43,44] As expected for proton transport, lower currents were observed when D_2O was used instead of H_2O to control the relative humidity conditions (**Figure 4**A). The measured KIE values provided, in addition, insight to the proton transport mechanisms.[34,43,44] The ratio between the conductance in H_2O and D_2O environments was found to be >1.4 for the entire relative humidity range. Such values indicate that the conductivity is dominated by the Grotthus proton transport mechanism. The ratio seems to decrease monotonically with the increase in the relative humidity from a large ratio of 2.0 at 40% RH to 1.4 at 70% relative humidity, suggesting increasing contribution of vehicle type proton transport to the conductivity with the increase in relative humidity, as could be expected. Quantitative assessment of the possible contribution of electrons to current flow was obtained by comparing the conductance of the $(KYY)_{ox}$ fiber films measured with proton transparent (palladium hydride) contacts and the conductance measured with electron transparent (palladium) electrodes (Figure 4B). Significantly higher currents were observed when palladium hydride contacts were used, further confirming that the charge transport by protons dominates the conductivity. As the relative humidity increases, the ratio between the

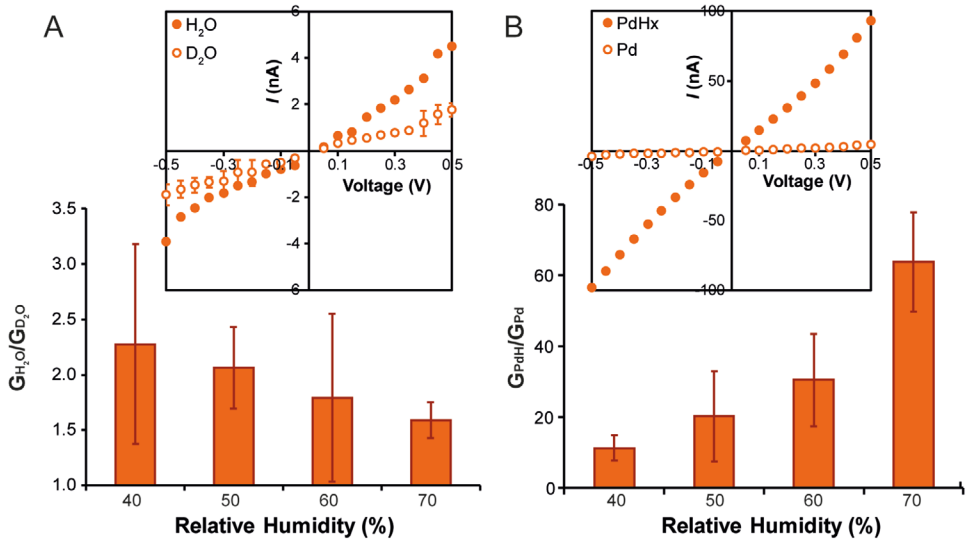

Figure 4. Nature of charge carriers in $(KYY)_{ox}$ films. A) Ratio of conductance (G) in H_2O/D_2O as a function of relative humidity. The inset shows I–V curves in H_2O and D_2O atmosphere at 60% RH, extracted using Pd contacts. B) The ratio of G of samples measured using PdHx/Pd contacts as a function of relative humidity. The inset shows I–V curves of the same sample using PdH_x and Pd contacts at 60% RH. I–Vs were obtained for devices with 10 µm gaps.

conductance measured with palladium hydride and palladium contacts increased from 10 at 40% relative humidity up to ≈60 at 70% RH, indicating that the dominance of proton charge carriers over the current flow increases with the humidity.

To summarize, we have demonstrated that enzymatic oxidation of a minimalistic self-assembling peptide containing two oxidizable tyrosines results in conductive supramolecular melanin-like fibers. While the oxidation of assembled fibers leads to controlled internal structural disorder, we show that the assemblies retain an overall fibrillar morphology and, to some extent, supramolecular order, which is important for their electric properties. This de novo design and control of supramolecular order/disorder enables high level of control of the 1D morphology of supramolecular melanin-like structures that present broadband UV–vis absorption and unprecedented high conductivity. The high conductivity of the oxidized supramolecular fibers at the mesoscale was found to be mediated mostly by proton transport via the Grotthus mechanism, with negligible electronic contribution. Thus, the simplicity of the building blocks utilized here and the emerging melanin-like functionality upon assembly and oxidation enables fundamental properties to be systematically studied and optimized, opening new opportunities in bioelectronics applications, especially in applications where large surface to volume ratio is required, for example in supercapacitors and batteries.

Supporting Information

Supporting Information is available from the Wiley Online Library or from the author.

Acknowledgements

S.M.M.R. and E.R. contributed equally to this work. This research was supported by the U.S. Air Force Office of Scientific Research (grant FA9550-19-1-0111) and by the Israel Science Foundation (grant No. 375/18). S.M.M.R. is a recipient of the BGU Kreitman School for post-doctorate fellowship. The authors thank O. Abarbanel, S. Panettieri, and Y. He (Live Imaging Facility at the Advanced Science Research Center, The Graduate Center CUNY) and S. A. McPhee (Nanoscience Initiative, ASRC, CUNY) for the help with the SHG imaging and LCMS analysis. Devices were fabricated at the Unit for Nanofabrication at the Hebrew University of Jerusalem.

Conflict of Interest

The authors declare no conflict of interest.

Keywords

melanin, peptides, proton conduction, self-assembly, supramolecular materials

Received: May 22, 2020
Revised: September 18, 2020
Published online: October 15, 2020

[1] M. Xiao, Y. Li, M. C. Allen, D. D. Deheyn, X. Yue, J. Zhao, N. C. Gianneschi, M. D. Shawkey, A. Dhinojwala, *ACS Nano* **2015**, *9*, 5454.
[2] N. Amdursky, E. D. Głowacki, P. Meredith, *Adv. Mater.* **2019**, *31*, 1802221.
[3] M. Sheliakina, A. Mostert, P. Meredith, *Mater. Horiz.* **2018**, *5*, 256.
[4] Y. J. Kim, W. Wu, S.-E. Chun, J. F. Whitacre, C. J. Bettinger, *Proc. Natl. Acad. Sci. USA* **2013**, *110*, 20912.
[5] F. G. Kapp, J. R. Perlin, E. J. Hagedorn, J. M. Gansner, D. E. Schwarz, L. A. O'Connell, N. S. Johnson, C. Amemiya, D. E. Fisher, U. Wölfle, *Nature* **2018**, *558*, 445.
[6] E. Dadachova, R. A. Bryan, X. Huang, T. Moadel, A. D. Schweitzer, P. Aisen, J. D. Nosanchuk, A. Casadevall, *PLoS One* **2007**, *2*, e457.

[7] M. d'Ischia, A. Napolitano, V. Ball, C.-T. Chen, M. J. Buehler, *Acc. Chem. Res.* **2014**, *47*, 3541.
[8] M. d'Ischia, A. Napolitano, A. Pezzella, P. Meredith, M. Buehler, *Angew. Chem., Int. Ed.* **2020**, *59*, 11196.
[9] Y. Liu, K. Ai, L. Lu, *Chem. Rev.* **2014**, *114*, 5057.
[10] P. Meredith, C. J. Bettinger, M. Irimia-Vladu, A. B. Mostert, P. E. Schwenn, *Rep. Prog. Phys.* **2013**, *76*, 034501.
[11] M. L. Tran, B. J. Powell, P. Meredith, *Biophys. J.* **2006**, *90*, 743.
[12] M. Sheliakina, A. B. Mostert, P. Meredith, *Adv. Funct. Mater.* **2018**, *28*, 1805514.
[13] J. McGinness, P. Corry, P. Proctor, *Science* **1974**, *183*, 853.
[14] A. B. Mostert, B. J. Powell, F. L. Pratt, G. R. Hanson, T. Sarna, I. R. Gentle, P. Meredith, *Proc. Natl. Acad. Sci. USA* **2012**, *109*, 8943.
[15] P. Baraldi, R. Capelletti, P. Crippa, N. Romeo, *J. Electrochem. Soc.* **1979**, *126*, 1207.
[16] A. B. Mostert, B. J. Powell, I. R. Gentle, P. Meredith, *Appl. Phys. Lett.* **2012**, *100*, 093701.
[17] J. Wünsche, Y. Deng, P. Kumar, E. D.i Mauro, E. Josberger, J. Sayago, A. Pezzella, F. Soavi, F. Cicoira, M. Rolandi, C. Santato, *Chem. Mater.* **2015**, *27*, 436.
[18] A. Lampel, R. Ulijn, T. Tuttle, *Chem. Soc. Rev.* **2018**, *47*, 3737.
[19] M. Amit, S. Yuran, E. Gazit, M. Reches, N. Ashkenasy, *Adv. Mater.* **2018**, *30*, 1707083.
[20] B. Sun, A. D. Ariawan, H. Warren, S. C. Goodchild, L. M. Ittner, A. D. Martin, *J. Mater. Chem. B* **2020**, *8*, 3104.
[21] A. Lampel, S. A. McPhee, H.-A. Park, G. G. Scott, S. Humagain, D. R. Hekstra, B. Yoo, P. W. J. M. Frederix, T.-D. Li, R. R. Abzalimov, S. G. Greenbaum, T. Tuttle, C. Hu, C. J. Bettinger, R. V. Ulijn, *Science* **2017**, *356*, 1064.
[22] P. W. J. M. Frederix, G. G. Scott, Y. M. Abul-Haija, D. Kalafatovic, C. G. Pappas, N. Javid, N. T. Hunt, R. V. Ulijn, T. Tuttle, *Nat. Chem.* **2015**, *7*, 30.
[23] M. A. Gebbie, W. Wei, A. M. Schrader, T. R. Cristiani, H. A. Dobbs, M. Idso, B. F. Chmelka, J. H. Waite, J. N. Israelachvili, *Nat. Chem.* **2017**, *9*, 473.
[24] H. Lee, S. M. Dellatore, W. M. Miller, P. B. Messersmith, *Science* **2007**, *318*, 426.
[25] A. Handelman, S. Lavrov, A. Kudryavtsev, A. Khatchatouriants, Y. Rosenberg, E. Mishina, G. Rosenman, *Adv. Opt. Mater.* **2013**, *1*, 875.
[26] L. C. Serpell, *Biochim. Biophys. Acta* **2000**, *1502*, 16.
[27] B. Hernández, Y.-M. Coïc, F. Pflüger, S. G. Kruglik, M. Ghomi, *J. Raman Spectrosc.* **2016**, *47*, 210.
[28] E. Vass, M. Hollósi, F. Besson, R. Buchet, *Chem. Rev.* **2003**, *103*, 1917.
[29] L. D. Barron, E. W. Blanch, I. H. McColl, C. D. Syme, L. Hecht, K. Nielsen, *Spectroscopy* **2003**, *17*, 101.
[30] D. Kurouski, R. P. Van Duyne, I. K. Lednev, *Analyst* **2015**, *140*, 4967.
[31] J. Bandekar, S. Krimm, *Proc. Natl. Acad. Sci. USA* **1979**, *76*, 774.
[32] S. Mondal, A. Thampi, M. Puranik, *J. Phys. Chem. B* **2018**, *122*, 2047.
[33] C. Zhong, Y. Deng, A. F. Roudsari, A. Kapetanovic, M. P. Anantram, M. Rolandi, *Nat. Commun.* **2011**, *2*, 476.
[34] M. Amit, S. Roy, Y. Deng, E. Josberger, M. Rolandi, N. Ashkenasy, *ACS Appl. Mater. Interfaces* **2018**, *10*, 1933.
[35] O. Silberbush, M. Amit, S. Roy, N. Ashkenasy, *Adv. Funct. Mater.* **2017**, *27*, 1604624.
[36] T.-F. Wu, B.-H. Wee, J.-D. Hong, *Adv. Mater.* **2015**, *2*, 1500203.
[37] J. Selberg, M. Jia, M. Rolandi, *PLoS One* **2019**, *14*, e0202713.
[38] B. Rosenberg, *Nature* **1962**, *193*, 364.
[39] M. Amit, S. Appel, R. Cohen, G. Cheng, I. W. Hamley, N. Ashkenasy, *Adv. Funct. Mater.* **2014**, *24*, 5873.
[40] O. Silberbush, M. Engel, I. Sivron, S. Roy, N. Ashkenasy, *J. Phys. Chem B* **2019**, *123*, 9882.
[41] R. S. Raja Rafidah, W. Rashmi, M. Khalid, W. Y. Wong, J. Priyanka, *Polymers* **2020**, *12*, 1061.
[42] R. A. Huggins, *Ionics* **2002**, *8*, 300.
[43] S. Ø. Stub, E. Vøllestad, T. Norby, *J. Phys. Chem C* **2017**, *121*, 12817.
[44] S. Miyoshi, Y. Akao, N. Kuwata, J. Kawamura, Y. Oyama, T. Yagi, S. Yamaguchi, *Chem. Mater.* **2014**, *26*, 5194.